Manuscript prepared for The Cryosphere
with version 2015/11/06 7.99 Copernicus papers of the LaTeX class copernicus.cls.
Date: 18 May 2016

Critical investigation of calculation methods for the elastic velocities in anisotropic ice polycrystals

A. Maurel[1], J.-F. Mercier[2], and M. Montagnat[3]

[1] Institut Langevin, CNRS, ESPCI ParisTech, 1 rue Jussieu, 75005 Paris, France
[2]Poems, CNRS, ENSTA ParisTech, INRIA, 828 boulevard des Maréchaux 91762 Palaiseau, France
[3]LGGE, CNRS, Université Grenoble Alpes, 38041 Grenoble, France.

Correspondence to: A. Maurel (agnes.maurel@espci.fr)

Abstract. Sonic logging measurements in ice core boreholes allow the determination of velocities of the elastic waves used as proxy for the variation of ice polycrystal anisotropy due to the texture (or fabric) evolution with depth. The idea beyond these measurements is to invert the elastic velocities to deduce the ice polycrystal anisotropy; this requires a model which links the elastic velocities to the ice texture. A classical model is based on the effective medium theory; the velocities are associated to elastic waves propagating in a homogeneous medium characterized by an average elasticity tensor. Alternatively, the velocity averaging model uses the average of the velocities in single crystals with different orientations.

In this paper, we show that the velocity average method is erroneous in the present context. This is demonstrated for waves propagating in a clustered polycrystal along the c-axis; two different shear wave velocities are obtained while a unique velocity is expected. This unphysical result is not recovered by Bennett (1968) although the velocity averaging method is used; we show that this is due to erroneous expressions of the shear wave velocities in single crystals, used as the starting point in the average process. Because of the weak elastic anisotropy of ice, the inversion from the measured velocities requires the use of an accurate model, models based on effective medium theory should be preferred.

1 Introduction

Wave propagation in glaciology most often is regarded in the context of seismic waves, see *e.g.* *Kohnen* (1974), *Blankenship et al.* (1987). More recently, the interest has been renewed with the idea of using in situ velocity measurements in boreholes in addition to usual thin section analysis, in order to measure the texture (fabric) anisotropy and its evolution with depth along deep ice cores. Sonic logging is based on the measure of the travel time of elastic waves propagating on a short distance (typically few meters). A campagne at Dome C has been performed using a classical sonic logger (*Gusmeroli et al.*, 2012). This campagne has revealed the sensitivity of the elastic velocities on the degree of anisotropy of ice polycrystals with a cluster-type texture (c-axis orientation clustered

around the vertical direction), that varies with depth. Nevertheless, the velocity changes are small, which requires low uncertainties in the measurements but also motivates the development of accurate models used in the inversion from the elastic velocities to the local ice anisotropy.

In a previous paper (*Maurel et al.*, 2015), we applied a classical model for wave propagation in polycrystals to the particular textures as found in ice recovered from deep ice cores, clusters with vertical transverse isotropy (VTI) and girdles with horizontal transverse isotropy (HTI). The model relies on the definition of an *effective medium* characterized by an averaged elasticity tensor defined at the scale of many grains. We presented a comparison with Bennett's predictions (*Bennett*, 1968) based on the velocity averaging method and illustrated the weak differences in the velocities predicted in the two models for ice clustered textures. Contrary to the effective medium theory, the velocity averaging method does not rely on a rigorous mathematical formalism. Thus, beyond the relative agreement observed for clustered textures, the correctness of the velocity averaging method can be questioned.

This is the goal of the present paper. We show that the velocity averaging method has an error in its fundamental assumption. This is demonstrated considering the cases of cluster and girdle textures with VTI in ice. It is found that a wave propagating along the vertical axis is associated to two different shear velocities, which is unphysical since the polarizations of the shear waves are in the plane of isotropy. In *Bennett* (1968) a unique expression of the shear velocity was obtained, starting with modified expressions of the two shear wave velocities in ice single crystals. The modification consisted in attributing symmetrical weights to both velocities in order to get the same value after velocity averaging. It results in a velocity value close to the harmonic mean of the unphysical velocities given by the direct use of the velocity averaging method. As previously said, the inversion procedure from the measured velocities to the ice texture needs an accurate model. This includes a model relying on a rigorous mathematical formalism able to describe the case of complex textures, beyond the simple case of VTI clusters. With regard to this requirement, the model based on effective medium theory appears more reliable.

2 Classical results on polycrystal effective anisotropy and wave propagation in anisotropic media

In this section, we recall classical results on (i) the propagation of elastic waves in a crystal or in a polycrystal characterized by a uniform elasticity tensor and (ii) on the elasticity tensor of polycrystals, regarded at the scale of many grains as an equivalent "single" crystal. This allows to introduce the notations that will be used in the sequel, and to clarify in a self consistent way some properties that will be needed.

2.1 Wave propagation in a uniform anisotropic medium – The Christoffel equation

In the following, we denote $\mathbf{x} = (x_1, x_2, x_3)$ the spatial coordinates, $\mathbf{u}(\mathbf{x}) = (u_1(\mathbf{x}), u_2(\mathbf{x}), u_3(\mathbf{x}))$ the elastic displacement vector, ρ the constant mass density and c_{abcd} the elasticity tensor being uniform in space. The case of a uniform c_{abcd} corresponds either to a single crystal or to a polycrystal thought as an effective medium and in this latter case, c_{abcd} characterizes the texture of the polycrystal. The propagation of monochromatic waves of frequency ω is described by the wave equation

$$\rho\omega^2 u_a(\mathbf{x}) + c_{abcd}\frac{\partial^2}{\partial x_b \partial x_c} u_d(\mathbf{x}) = 0, \tag{1}$$

with $a = 1, 2, 3$ and and where repeated indices mean summation (Einstein convention). Denoting $\mathbf{k} = k\mathbf{n}$ the wavevector (k is the wavenumber) with $\mathbf{n} = (n_1, n_2, n_3)$ the unitary vector along $\mathbf{k}$, the elastic displacement reads $u_a(\mathbf{x}) = U_a e^{i\mathbf{k}.\mathbf{x}}$ leading to $\rho\omega^2 U_a - k^2 c_{abcd} n_b n_c U_d = 0$ for $a = 1, 2, 3$. This system of equations admits non zero solution for (U_1, U_2, U_3) if the determinant of the matrix $\rho\omega^2\delta_{ad} - k^2 c_{abcd} n_b n_c$ vanishes (δ_{ab} is the Kronecker delta). One gets the dispersion relation which links k and ω; equivalently, introducing the phase velocity $V = \omega/k$, we get the classical form of the Christoffel equation

$$\text{Det}\left[\rho V^2 \delta_{ad} - c_{abcd} n_b n_c\right] = 0. \tag{2}$$

The Christoffel equation admits in general three solutions $V = V_P, V_{SH}, V_{SV}$ which are the elastic velocities of the longitudinal wave and the two transverse waves (P, SH and SV stand for pressure wave, shear horizontal and shear vertical waves). It is important to stress at this point that the three values of V^2 being the eigenvalues of the matrix $c_{abcd} n_b n_c/\rho$, they do not depend on the particular frame $(\mathbf{e}_1, \mathbf{e}_2, \mathbf{e}_3)$ used to express c_{abcd}. To the contrary, the eigenvectors (U_1, U_2, U_3) associated to the eigenvalues obviously depend on the frame where they are expressed.

2.2 Elasticity tensor of the polycrystal resulting from anisotropy from grain to grain

In the previous section, we have considered the uniform elasticity tensor of a polycrystal. This elasticity tensor is derived from the characteristics of the grains which compose the polycrystal. For ice, each grain is composed of the same single crystal with hexagonal symmetry being characterized by its elasticity tensor c^0_{ijkl}, written in terms of C^0_{IJ} in the Voigt's notation (*Voigt*, 1928). The superscript 0 refers to an elasticity tensor expressed in the frame of its principal axes, with the c-axis being oriented along $\mathbf{e}_3$, hereafter referred as the vertical axis. The Voigt's matrix C^0 (with elements C^0_{IJ},

$I = 1, \ldots 6$ and $J = 1, \ldots 6$) reads

$$\mathsf{C}^0 = \begin{pmatrix} A & A-2N & F & 0 & 0 & 0 \\ A-2N & A & F & 0 & 0 & 0 \\ F & F & C & 0 & 0 & 0 \\ 0 & 0 & 0 & L & 0 & 0 \\ 0 & 0 & 0 & 0 & L & 0 \\ 0 & 0 & 0 & 0 & 0 & N \end{pmatrix}, \tag{3}$$

with the standard notations

$$\begin{cases} c_{ijk\ell} \to C_{IJ}, \\ \text{for} \quad (i,j) \to I, \quad (k,l) \to J, \\ \text{and} \quad (1,1) \to 1, (2,2) \to 2, (3,3) \to 3, \\ \qquad (3,2), (2,3) \to 4, (3,1), (1,3) \to 5, (1,2), (2,1) \to 6. \end{cases} \tag{4}$$

For an arbitrary direction of the c-axis (Fig. 1)

$$\hat{\mathbf{c}} = (\sin\theta\cos\varphi, \sin\theta\sin\varphi, \cos\theta), \tag{5}$$

the elasticity tensor c_{abcd} is deduced from c^0_{ijkl} following

$$c_{abcd} = R_{ia} R_{jb} R_{kc} R_{ld} c^0_{ijk\ell}, \tag{6}$$

with R the rotation matrix (with elements R_{ij})

$$\mathsf{R} \equiv \begin{pmatrix} \cos\theta\cos\varphi & \cos\theta\sin\varphi & -\sin\theta \\ -\sin\varphi & \cos\varphi & 0 \\ \sin\theta\cos\varphi & \sin\theta\sin\varphi & \cos\theta \end{pmatrix}. \tag{7}$$

c_{abcd} depends on (θ, φ) which are the usual angles in spherical coordinates.

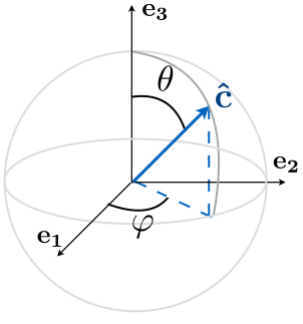

Figure 1. Spherical angles (φ, θ) used for the orientation of the c-axis, ($\hat{\mathbf{c}}$ is an unitary vector).

The anisotropy at the macroscopic scale (at the scale of many grains) results from the many (or few) possible orientations of the c-axis in each grain. This distribution of c-axes is defined by a

probability distribution function $p(\theta,\varphi)$ satisfying

$$\int \mathrm{d}\Omega\, p(\theta,\varphi) = 1, \quad \text{with } \mathrm{d}\Omega\ = \sin\theta\ \mathrm{d}\theta\mathrm{d}\varphi. \tag{8}$$

The elasticity tensor c^{eff}_{ijkl} and the associated Voigt's matrix C^{eff}_{IJ} of the polycrystal can be calculated by means of the average of the elasticity tensors of the grains following

$$c^{\text{eff}}_{ijkl} = \int \mathrm{d}\Omega\ p(\varphi,\theta) c_{ijkl}, \quad C^{\text{eff}}_{IJ} = \int \mathrm{d}\Omega\ p(\varphi,\theta) C_{IJ}, \tag{9}$$

with the same index convention, Eq. (4), between the elasticity tensor c^{eff}_{ijkl} and the Voigt matrix C^{eff}_{IJ}. For VTI textures, the direction of the axis of anisotropy is given by the effective c-axis, denoted $\hat{\mathbf{c}}^{\text{eff}}$.

For the numerical application, we will use the elastic constants as derived by *Bennett* (1968):

$$\text{Ice single crystal} \begin{cases} A = 14.06 \times 10^9\ \text{N.m}^{-2},\ C = 15.24 \times 10^9\ \text{N.m}^{-2},\ L = 3.06 \times 10^9\ \text{N.m}^{-2}, \\ N = 3.455 \times 10^9\ \text{N.m}^{-2},\ F = 5.88 \times 10^9\ \text{N.m}^{-2},\ \rho = 917\ \text{kg/m}^3. \end{cases} \tag{10}$$

3 Elastic wave velocities in the velocity averaging method and velocities of the effective medium for VTI textures

In this section, we compare the elastic velocities obtained from the velocity averaging method, as used in *Bennett* (1968); *Gusmeroli et al.* (2012); *Vélez et al.* (2016), and the elastic velocities obtained from the effective medium theory. The two approaches are as follow

Velocities from the velocity averaging method

First, solve the Christoffel equation for given (θ,φ) :

$$V(\theta,\varphi) = V_P, V_{SV}, V_{SH} \text{ are the roots of } \text{Det}\left[\rho V^2 \delta_{il} - c_{ijkl} n_j n_k\right],$$

Then compute the average of the slowness, from which: $V^{\text{av}} = \left[\int \mathrm{d}\Omega\, p(\theta,\varphi) V^{-1}(\theta,\varphi)\right]^{-1}$.

(11)

Velocities of the effective medium

First, compute the effective elasticity tensor: $c^{\text{eff}}_{ijkl} = \int \mathrm{d}\Omega\, p(\theta,\varphi) c_{ijkl}$,

Then, solve the Christoffel equation:

$$V = V^{\text{eff}}_P, V^{\text{eff}}_{SV}, V^{\text{eff}}_{SH} \text{ are the roots of Det} \left[\rho V^2 \delta_{il} - c^{\text{eff}}_{ijkl} n_j n_k\right].$$

(12)

Below, we report examples of VTI textures for which the velocity averaging method leads to inconsistent results. In such media and for a wave propagating along the vertical direction $\mathbf{e}_3$, the shear displacements are in the plane $(\mathbf{e}_1, \mathbf{e}_2)$, that is in the plane where the response of the polycrystal is isotropic. Thus, there is a unique shear velocity in this particular case ($V_{SV} = V_{SH}$).

Two examples of VTI structures will be presented and the propagation along the vertical direction is considered. The first structure is artificial, with a c-axis having a unique $\theta = \theta_0$ value in $[0, \pi/2]$ (and $\varphi \in [0,\ 2\pi]$), but it allows for explicit expressions of the velocities in both approaches. It could be seen as a girdle with VTI, (*Azuma and Goto-Azuma*, 1996) with a single zenith angle θ_0, Fig. 2. The second example corresponds to a cone representative of clustered textures measured along ice cores (*Gusmeroli et al.*, 2012; *Diez and al.*, 2015), with $\theta \in [0,\ \theta_0]$ (and $\varphi \in [0,\ 2\pi]$) and is studied numerically, Fig. 3.

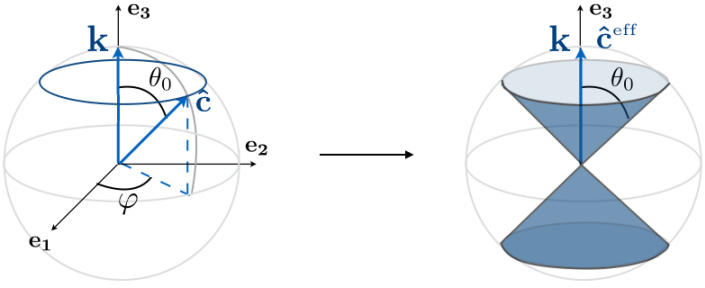

(a) (b)

Figure 2. First configuration of a VTI girdle with a single zenith angle θ_0. (a) shows a typical c-axis $\hat{\mathbf{c}} = (\sin\theta_0\cos\varphi, \sin\theta_0\sin\varphi, \cos\theta_0)$ within one grain, with a constant θ_0, and φ varies randomly from grain to grain. (b) shows the resulting VTI texture of the polycrystal at the macroscopic scale. $\hat{\mathbf{c}}^{\text{eff}}$ is the effective c-axis.

3.1 Wave propagation along the vertical axis in a polycrystal with VTI

We consider a wave propagating along the vertical axis, thus $\mathbf{k} = (0, 0, k)$, in a polycrystal with VTI, Figs. 2 and 3. The VTI structures allow for $\varphi \in [0,\ 2\pi]$ from which the probability distribution does not depend on φ. Thus, the distribution of c-axes is given by probability distribution functions of the form

$$p(\theta, \varphi) = \frac{P_{\theta_0}(\theta)}{2\pi}, \quad \text{with} \int_0^{\pi/2} \mathrm{d}\theta \sin\theta P_{\theta_0}(\theta) = 1. \tag{13}$$

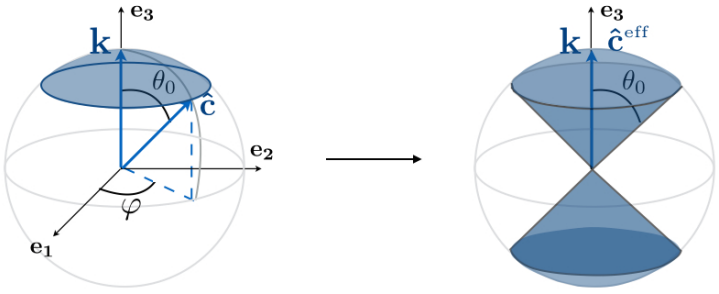

(a) (b)

Figure 3. Second configuration of the usual VTI clustered texture. (a) shows a typical c-axis $\hat{\mathbf{c}} = (\sin\theta\cos\varphi, \sin\theta\sin\varphi, \cos\theta)$ within one grain, θ varies in $[0, \theta_0]$ and φ varies randomly from grain to grain. (b) shows the resulting clustered, VTI, texture of the polycrystal at the macroscopic scale. $\hat{\mathbf{c}}^{\text{eff}}$ is the effective c-axis.

3.1.1 Velocities from the velocity averaging method

In this method, we first derive the velocities in a grain, and this is done without lack of generality for a wave propagating along $\mathbf{e}_3$. The Christoffel equation, Eq. (2) with $n_b = \delta_{b3}$ (same for n_c) simplifies to

$$\begin{vmatrix} \rho V^2 - C_{55} & -C_{45} & -C_{35} \\ -C_{45} & \rho V^2 - C_{44} & -C_{34} \\ -C_{35} & -C_{34} & \rho V^2 - C_{33} \end{vmatrix} = 0, \tag{14}$$

where the C_{IJ} is derived from c_{ijkl} in Eq. (6), for a c-axis given by Eq. (5)

$$\begin{cases} C_{33} = A\mathrm{s}\theta^4 + 2(2L+F)\mathrm{s}\theta^2\mathrm{c}\theta^2 + C\mathrm{c}\theta^4, \\ C_{44} = (A+C-2F)\mathrm{s}\theta^2\mathrm{c}\theta^2\mathrm{s}\varphi^2 + L\left[\mathrm{s}\varphi^2(\mathrm{c}\theta^2-\mathrm{s}\theta^2)^2 + \mathrm{c}\theta^2\mathrm{c}\varphi^2\right] + N\mathrm{s}\theta^2\mathrm{c}\varphi^2, \\ C_{55} = (A+C-2F)\mathrm{s}\theta^2\mathrm{c}\theta^2\mathrm{c}\varphi^2 + L\left[\mathrm{c}\varphi^2(\mathrm{c}\theta^2-\mathrm{s}\theta^2)^2 + \mathrm{c}\theta^2\mathrm{s}\varphi^2\right] + N\mathrm{s}\theta^2\mathrm{s}\varphi^2, \\ C_{34} = -\mathrm{s}\varphi\mathrm{s}\theta\mathrm{c}\theta\left[A\mathrm{s}\theta^2 - C\mathrm{c}\theta^2 + (2L+F)(1-2\mathrm{s}\theta^2)\right], \\ C_{35} = -\mathrm{c}\varphi\mathrm{s}\theta\mathrm{c}\theta\left[A\mathrm{s}\theta^2 - C\mathrm{c}\theta^2 + (2L+F)(1-2\mathrm{s}\theta^2)\right], \\ C_{45} = \mathrm{s}\varphi\mathrm{c}\varphi\mathrm{s}\theta^2\left[(A+C-2F)\mathrm{c}\theta^2 + L(1-4\mathrm{c}\theta^2) - N\right], \end{cases} \tag{15}$$

and we have used the notations $\mathrm{c}\varphi \equiv \cos\varphi$, $\mathrm{s}\varphi \equiv \sin\varphi$, $\mathrm{s}\theta \equiv \sin\theta$ and $\mathrm{c}\theta \equiv \cos\theta$. The determinant, Eq. (14), can be calculated and we get the roots ρV^2

$$\begin{cases} \rho V^2 = \left(L\mathrm{c}\theta^2 + N\mathrm{s}\theta^2\right), \\ (\rho V^2)^2 + \left(A\mathrm{s}\theta^2 + C\mathrm{c}\theta^2 + L\right)\rho V^2 - F^2\mathrm{s}\theta^2\mathrm{c}\theta^2 + AC\mathrm{s}\theta^2\mathrm{c}\theta^2 + AL\mathrm{s}\theta^4 + CL\mathrm{c}\theta^4 - 2FL\mathrm{s}\theta^2\mathrm{c}\theta^2 = 0. \end{cases} \tag{16}$$

The first root corresponds to a pure shear wave polarized in a direction perpendicular to both $\mathbf{k}$ and $\hat{\mathbf{c}}$, referred as SH-wave. The two roots of the second equation are associated to the so-called quasi shear

and quasi longitudinal waves, being coupled. The directions of polarization of the three waves are orthogonal (because the determinant is associated to a symmetric matrix) but the quasi longitudinal wave is in general not along $\mathbf{e}_3$ and the quasi shear wave is in general not in the $(\mathbf{e}_1, \mathbf{e}_2)$ plane. More explicitly, the three velocities read

$$\left\{\begin{array}{l} \rho V_{SH}^2 = L\mathrm{c}\theta^2 + N\mathrm{s}\theta^2, \\ \rho V_{SV}^2 = \dfrac{1}{2}\Big[C + L + (A-C)\mathrm{s}\theta^2 - \sqrt{D}\Big], \\ \rho V_P^2 = \dfrac{1}{2}\Big[C + L + (A-C)\mathrm{s}\theta^2 + \sqrt{D}\Big], \end{array}\right. \tag{17}$$

with $\quad D \equiv \big[A\mathrm{s}\theta^2 - C\mathrm{c}\theta^2\big]\big[A\mathrm{s}\theta^2 - C\mathrm{c}\theta^2 + 2L(\mathrm{c}\theta^2 - \mathrm{s}\theta^2)\big] + 4\mathrm{s}\theta^2\mathrm{c}\theta^2(F^2 + 2FL) + L^2.$

These are the expressions of the velocities in a single grain with a c-axis forming an angle θ with $\mathbf{k}$.

The second step in the velocity averaging method can be applied

$$\frac{1}{V^{\mathrm{av}}(\theta_0)} = \int_0^{2\pi} \mathrm{d}\varphi \int_0^{\pi/2} \mathrm{d}\theta\, \sin\theta\, p(\theta,\varphi) V^{-1}(\theta,\varphi) = \int_0^{\pi/2} \mathrm{d}\theta\, \sin\theta\, P_{\theta_0}(\theta) V^{-1}(\theta), \tag{18}$$

for $V = V_{SH}, V_{SV}, V_P$ taken from Eqs. (17). These last averages depend further on $P_{\theta_0}(\theta)$.

3.1.2 Velocities of the effective medium

With the probability function given by Eq. (13), the effective medium is characterized by a Voigt matrix

$$C_{IJ}^{\mathrm{eff}}(\theta_0) = \int_0^{2\pi} \frac{\mathrm{d}\varphi}{2\pi} \int_0^{\pi/2} \mathrm{d}\theta\, C_{IJ}(\theta,\varphi) \sin\theta\, P_{\theta_0}(\theta). \tag{19}$$

The Voigt matrix $C_{IJ}(\theta,\varphi)$ has 21 non-zero coefficients. Averaging $C_{IJ}(\theta,\varphi)$ over $\varphi \in [0,\, 2\pi]$ makes 15 of them to vanish, and the resulting Voigt matrix has VTI symmetry, as expected, see Eqs. (A2)-(A3) in *Maurel et al.* (2015). The remaining integrations over θ depend on $P_{\theta_0}(\theta)$.

Next, the velocities of the elastic waves propagating along the axis $\mathbf{e}_3$ can be derived by solving the Christoffel equation, Eq. (2) with $C_{IJ} \to C_{IJ}^{\mathrm{eff}}$. We get

$$\left|\begin{array}{ccc} \rho V^2 - C_{44}^{\mathrm{eff}}(\theta_0) & 0 & 0 \\ 0 & \rho V^2 - C_{44}^{\mathrm{eff}}(\theta_0) & 0 \\ 0 & 0 & \rho V^2 - C_{33}^{\mathrm{eff}}(\theta_0) \end{array}\right| = 0, \tag{20}$$

and we report below the intermediate result on C_{33} and C_{44} after φ-averaging, from Eq. (15),

$$\left\{\begin{array}{l} \langle C_{33}\rangle_\varphi(\theta) = A\mathrm{s}\theta^4 + 2(2L+F)\mathrm{s}\theta^2\mathrm{c}\theta^2 + C\mathrm{c}\theta^4, \\ \langle C_{44}\rangle_\varphi(\theta) = L\mathrm{c}\theta^2 + N\mathrm{s}\theta^2, \end{array}\right. \tag{21}$$

afterwards

$$C_{IJ}^{\mathrm{eff}}(\theta_0) = \int \mathrm{d}\theta\, \langle C_{IJ}\rangle_\varphi(\theta) \sin\theta\, P_{\theta_0}(\theta). \tag{22}$$

The resulting effective velocities read

$$\begin{cases} V_P^{\text{eff}} = \sqrt{C_{33}^{\text{eff}}(\theta_0)/\rho}, \\ V_S^{\text{eff}} = \sqrt{C_{44}^{\text{eff}}(\theta_0)/\rho}. \end{cases} \tag{23}$$

The longitudinal wave has a velocity associated to the polarization along $\mathbf{e}_3$; more importantly for the present demonstration, the two transverse waves have polarizations in the $(\mathbf{e}_1, \mathbf{e}_2)$ plane and they are associated to the same velocity.

3.2 Examples of the velocity averaging method for polycrystals with VTI

3.2.1 Example 1: the VTI girdle with a single zenith angle θ_0

The first configuration is shown in Fig. 2. All the grains within the polycrystal have the same angle $\theta = \theta_0$ but different φ randomly distributed in $[0, 2\pi]$, whence

$$P_{\theta_0}(\theta) = \frac{\delta(\theta - \theta_0)}{\sin\theta_0}. \tag{24}$$

The velocities obtained from the velocity averaging method, Sec. 3.1.1, are obtained with V in Eqs. (17) and Eqs. (18) and (24), leading to

$$\begin{cases} V_{SH}^{\text{av}} = \sqrt{\dfrac{L\text{c}\theta_0^2 + N\text{s}\theta_0^2}{\rho}}, \\ V_{SV}^{\text{av}} = \sqrt{\dfrac{C + L + (A - C)\text{s}\theta_0^2 - \sqrt{D}}{2\rho}}, \\ V_P^{\text{av}} = \sqrt{\dfrac{C + L + (A - C)\text{s}\theta_0^2 + \sqrt{D}}{2\rho}}, \end{cases} \tag{25}$$

with $\quad D \equiv \left[A\text{s}\theta_0^2 - C\text{c}\theta_0^2\right]\left[A\text{s}\theta_0^2 - C\text{c}\theta_0^2 + 2L(\text{c}\theta_0^2 - \text{s}\theta_0^2)\right] + 4\text{s}\theta_0^2\text{c}\theta_0^2(F^2 + 2FL) + L^2.$

These velocities are reported in Figs. 4(a) (red curves) and they will be discussed later. We now derive the two shear and transverse velocities of the effective medium, Sec. 3.1.2, which are given by Eqs. (23) with $C_{IJ}^{\text{eff}}(\theta_0) = \int \text{d}\theta \, \langle C_{IJ} \rangle_\varphi(\theta) \sin\theta \, P_{\theta_0}(\theta)$, and Eqs. (21) and (24). We get

$$\begin{cases} V_P^{\text{eff}} = \sqrt{\dfrac{1}{\rho}\left[A\text{s}\theta_0^4 + 2(2L + F)\text{s}\theta_0^2\text{c}\theta_0^2 + C\text{c}\theta_0^4\right]}, \\ V_S^{\text{eff}} = \sqrt{\dfrac{1}{2\rho}\left[(A + C - 2F)\text{s}\theta_0^2\text{c}\theta_0^2 + L(4\text{s}\theta_0^4 - 5\text{s}\theta_0^2 + 2) + N\text{s}\theta_0^2\right]}, \end{cases} \tag{26}$$

and these velocities are reported in black lines in Figs. 4(a).

3.2.2 Example 2: the VTI clustered texture with opening angle θ_0

This texture is shown in Fig. 3. It corresponds to

$$P_{\theta_0}(\theta) = \frac{H_{\theta_0}(\theta)}{1 - \cos\theta_0}, \tag{27}$$

where H_{θ_0} is the rectangular function, equals unity for $0 \leq \theta \leq \theta_0$, zero otherwise. The velocities $(V_{SH}^{\text{av}}, V_{SV}^{\text{av}}, V_P^{\text{av}})$ in the velocity averaging method, Sec. 3.1.1, cannot be calculated analytically in this case. The averages on θ in Eq. (18) are performed numerically (with Eqs. (17) and (27)), and they are shown in red lines in Fig. 4(b).

The velocities of the effective medium ($V_S^{\text{eff}}, V_P^{\text{eff}}$, Sec. 3.1.2) are calculated as previously, using Eqs. (21) to (23), with Eq. (27), and we get

$$\text{Cluster} \begin{cases} V_S^{\text{eff}} = \sqrt{\dfrac{(L+N)}{2\rho} + \dfrac{[2(A+C)-4F-3L-5N]}{30\rho}X - \dfrac{[(A+C)-2(2L+F)]}{10\rho}Y} \\ V_P^{\text{eff}} = \sqrt{\dfrac{A}{\rho} + \dfrac{[-7A+3C+4(2L+F)]}{15\rho}X + \dfrac{[A+C-2(2L+F)]}{5\rho}Y} \end{cases} \tag{28}$$

with $X \equiv 1 + \cos\theta_0 + \cos^2\theta_0$ and $Y \equiv \cos^3\theta_0 + \cos^4\theta_0$. These results are shown in black lines in Fig. 4(b).

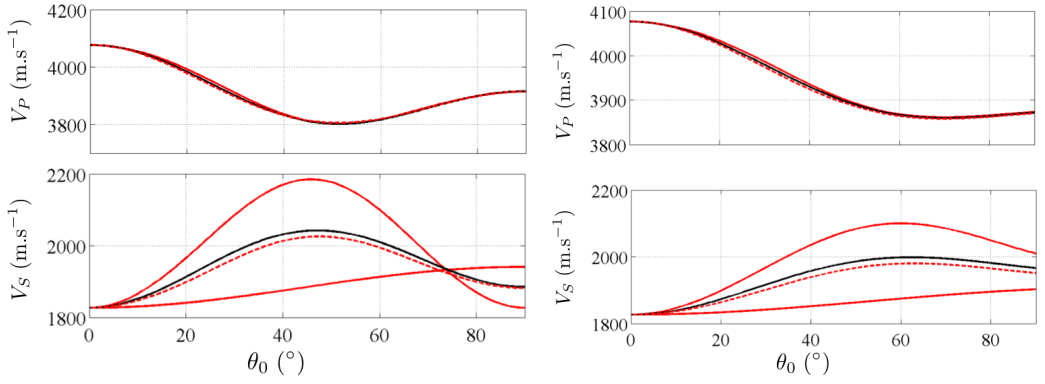

(a) (b)

Figure 4. Illustration of the inconsistency of the velocity averaging method for the two VTI textures shown in (a) Fig. 2 and (b) Fig. 3 The velocities V_P and V_S are reported as a function of θ_0, from the effective medium theory (black curves) and from the velocity averaging method (plain red lines). The dotted red lines show the shear wave velocity from Bennett's expression, close to the harmonic mean of the two unphysical shear wave velocities in plain red line.

Let us now discuss Figs. 4. Black lines correspond to the velocities V_P^{eff} and V_S^{eff} and as previously said, a unique velocity V_S^{eff} is found from the effective medium theory, by construction. Red lines correspond to the velocities V_P^{av} and $(V_{SH}^{\text{av}}, V_{SV}^{\text{av}})$ from the velocity averaging method. The discrepancy is incidental for the longitudinal wave velocity and does not allow to discriminate between the two methods. The important result is that we find two distinct shear wave velocities using the velocity averaging method, which is unphysical in the present case.

4 Comment on Bennett's derivation of the velocities in the usual clustered texture

Bennett (1968) presented a calculation of the elastic velocities in the VTI cluster (Fig. 3), and he obtained a unique expression of the shear velocity. This result is in contradiction with the calculations performed in the previous section and reported in plain red lines in Fig. 4. To understand this discrepancy, we analyze the derivation proposed in *Bennett* (1968).

4.1 Bennett's calculations in *Bennett* (1968)

Bennett starts with the slownesses in a single crystal

$$S = 1/V,$$

given by

$$\begin{cases} S_1 = S_P \simeq a_1 - b_1 \cos 4\theta - c_1 \cos 2\theta, \\ S_2 = S_{SV} \simeq a_2 + b_2 \cos 4\theta, \\ S_3 = S_{SH} \simeq a_3 + b_3 \cos 2\theta, \end{cases} \tag{29}$$

where $(a_1, a_2, a_3, b_2, b_3)$ are constant for ice. The above expressions are close to the Thomsen approximations (*Thomsen*, 1986) and they correspond to approximate expressions of the inverses of the velocities in single crystals given in Eqs. (17). In the above expressions, θ is the angle $(\mathbf{k}, \hat{\mathbf{c}})$ (Fig. 5(a)). Bennett used a different frame where neither $\mathbf{k}$ nor $\hat{\mathbf{c}}$ are along $\mathbf{e}_3$. In this frame, new multiple angles are defined (Fig. 5(b)): $\sigma \equiv (\mathbf{k}, \mathbf{e}_3)$, $\theta = (\hat{\mathbf{c}}, \mathbf{e}_3)$ and $\hat{\theta} \equiv (\mathbf{k}, \hat{\mathbf{c}})$. An additional angle

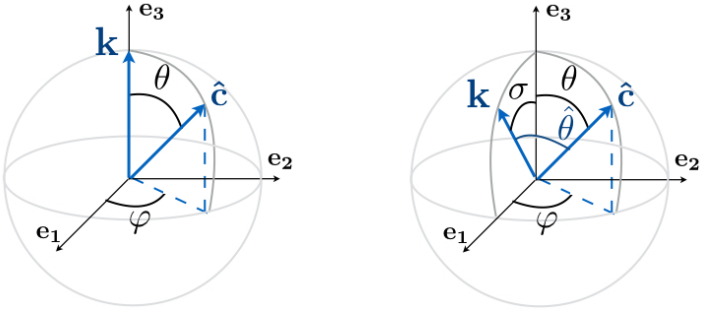

(a) (b)

Figure 5. (a) System of angles used in Bennett's calculations. $\hat{c}$ is given by (φ, θ) and $\mathbf{k}$ is given by σ, being otherwise in the $(\mathbf{e}_1, \mathbf{e}_3)$ plane. The extra angle $\hat{\theta}$ denotes the angle between $\mathbf{k}$ and $\hat{\mathbf{c}}$, thus $\cos\hat{\theta} = \sin\sigma\cos\varphi\sin\theta + \cos\sigma\cos\theta$. (b) Particular case of the Bennett configuration, for $\sigma = 0$; in this case, $\hat{\theta} = \theta$.

$\hat{\varphi}$, not represented in Fig. 5(a), between the planes $(\mathbf{k}, \mathbf{e}_3)$ and $(\mathbf{k}, \hat{\mathbf{c}})$ is used. Next, an ensemble of relations between the different angles are derived, among which $\cos\hat{\theta} = \sin\sigma\cos\varphi\sin\theta + \cos\sigma\cos\theta$

and

$$\begin{cases} \sin^2\hat{\varphi} = \dfrac{\sin^2\varphi\sin^2\theta}{\sin^2\hat{\theta}}, \\ \cos^2\hat{\varphi} = \dfrac{(\cos\sigma\cos\varphi\sin\theta - \sin\sigma\cos\theta)^2}{\sin^2\hat{\theta}} \end{cases} \tag{30}$$

and these relations are correct, for instance if $\sigma = 0$, then $\hat{\theta} = \theta$ and $\hat{\varphi} = \varphi$, as expected. Next, it is said that the slowness of the wave depends on $\hat{\varphi}$ following

$$\begin{cases} S_P = S_1, \\ S_{SV} = S_2\cos^2\hat{\varphi} + S_3\sin^2\hat{\varphi}, \\ S_{SH} = S_2\sin^2\hat{\varphi} + S_3\cos^2\hat{\varphi}. \end{cases} \tag{31}$$

This is announced by Bennett as an intuitive approximation. Obviously (see Eqs. (30)), $\hat{\varphi}$ can vary while $\hat{\theta}$ remains constant, from which the above equations pretend that the velocity of the shear waves depends on something else than on $\hat{\theta}$ only, and this is incorrect, from Eq. (29). More explicitly, using $\sigma = 0$ (thus, $\hat{\theta} = \theta$, $\hat{\varphi} = \varphi$) in the Eq. (31) and using Eqs. (29)-(30), we get

$$\begin{cases} S_{SV} = (a_2 + b_2) - 8b_2\cos^2\varphi\cos^2\theta\sin^2\theta - 2b_3\sin^2\varphi\sin^2\theta, \\ \\ S_{SH} = (a_2 + b_2) - 8b_2\sin^2\varphi\cos^2\theta\sin^2\theta - 2b_3\cos^2\varphi\sin^2\theta, \end{cases} \tag{32}$$

see Eqs. (5-15) in *Bennett* (1968). These expressions for the velocities in single crystal contain an unphysical dependence of φ and they do not agree with their original expressions, Eqs (29). The modification in Eqs. (31) when compared to the original expressions consists in attributing symmetrical weights to both S_1 and S_2 in order to get a same value after velocity averaging. Bennett's results are reported in dotted red lines in Figs. 4. As expected, the shear wave velocity appears to be close to the harmonic mean of the two unphysical velocities (resulting from the velocity averaging calculation). The velocity of the P-wave, being not modified by artificial weights, remains the same.

It is difficult to anticipate the consequences of such approach for other textures, since the weights in Eqs. (31) have to be chosen anticipating an expecting result after velocity averaging. The intuition that one can have for simple textures may become hazardous when complex textures are sought.

5 Conclusions

In this paper, we have proposed a critical analysis of the velocity averaging method as used recently in the post treatment of the velocities deduced from borehole sonic logging measurements. We have illustrated the error in the fundamental assumption of this method. This has been done in the case of simple VTI textures for which the error leads to an unphysical result, thus allows for a clear demonstration. For VTI textures, Bennett circumvented this problem by using weighted forms of the shear wave velocities (*Bennett*, 1968). The method is clever but it requires to anticipate good guesses of the weights, which may become difficult for complex structures.

The sonic logging measurements are sought as a proxy of the ice polycrystal anisotropy. Beyond the case of cluster textures, complex textures could be characterized by such methods (or at least transitions between various textures with depth). On the one hand, the anisotropy of the ice single crystal is weak, and thus, the anisotropy of ice polycrystals is even weaker. But on the other hand, ice polycrystals as recovered in boreholes are reasonably free of impurities when compared to most of the materials concerned by such sonic measurements. The recent campaign at Dome C has revealed the feasibility of such measurements (*Gusmeroli et al.*, 2012). Nowadays, commercial loggers allow for precise velocity measurements. In parallel, the characterization of the physical properties of ice single crystal and of the dependences of these properties with pressure and temperature reaches precisions of the order of few percents. This increase in the precision makes possible the inverse problem, from the measured velocities to the ice texture but the model needed in this inversion has to be accurate as well. With respect to this requirement, a rigorous model as the model based on the effective medium theory appears as a good candidate.

References

Azuma, N., and Goto-Azuma, K. (1996). An anisotropic flow law for ice-sheet ice and its implications. Annals of Glaciology, 23, 202-208.

Bennett H.F. 1968 An investigation into velocity anisotropy through measurements of ultrasonic wave velocities in snow and ice cores from Green- land and Antarctica. Ph.D. thesis, University of Wisconsin, Madison, 1968.

Blankenship, D. D., Bentley, C. R., Rooney, S. T., and Alley, R. B. (1987). Till beneath Ice Stream B: 1. Properties derived from seismic travel times. Journal of Geophysical Research: Solid Earth (1978 - 2012), 92(B9), 8903-8911.

Diez, A., and Eisen, O. (2015). Seismic wave propagation in anisotropic ice-Part 1: Elasticity tensor and derived quantities from ice-core properties. The Cryosphere, 9(1), 367-384.

Diez, A., Eisen, O., Hofstede, C., Lambrecht, A., Mayer, C., Miller, H., Weikusat, I. (2015). Seismic wave propagation in anisotropic ice-Part 2: Effects of crystal anisotropy in geophysical data. The Cryosphere, 9(1), 385-398.

Diez, A., and Eisen, O. (2015). Seismic wave propagation in anisotropic ice-Part 1: Elasticity tensor and derived quantities from ice-core properties. The Cryosphere, 9(1), 367-384.

Gusmeroli, A., Pettit, E. C., Kennedy, J. H., and Ritz, C. (2012). The crystal fabric of ice from full?waveform borehole sonic logging. Journal of Geophysical Research: Earth Surface (2003-2012), 117(F3).

Keller JB. 1964 Stochastic Equations and Wave Propagation in Random Media. in *Proceedings of the 16th Symposium on Applied Mathematics* (AMS, New York, 1964) 145-179.

Karal Jr FC, Keller JB. 1964 Elastic, Electromagnetic and Other Waves in Random medium. *J. Math. Phys.* **5** 537-547.

Kohnen, H. (1974). The temperature dependence of seismic waves in ice. J. Glaciol, 13(67), 144-147.

Maurel, A., Lund, F., and Montagnat, M. (2015, May). Propagation of elastic waves through textured polycrystals: application to ice. In Proceedings of the Royal Society of London A: Mathematical, Physical and Engineering Sciences (Vol. 471, No. 2177, p. 20140988). The Royal Society.

Middya, T. R., Paul, M., and Basu, A. N. (1986). Multiple scattering theoretical and computer simulated dynamic model approaches to effective elastic properties of randomly disordered composites. Journal of applied physics, 59(7), 2376-2381.

Thomsen GW. 1986 Weak elastic anisotropy. *Geophysics* **15** 1954-1966.

Thorsteinsson T. 1990 Textures and fabrics in bottom silty ice from the Dye 3 ice core. University of Copenhagen, MS thesis.

Voigt W. 1928 Lehrbuch der Kristallphysik, reprint of the 1st edn. Leipzig: Teubner.

Vélez, J. A., Tsoflias, G. P., Black, R. A., Van der Veen, C. J. and Anandakrishnan, S. (2016). Distribution of preferred ice crystal orientation determined from seismic anisotropy: Evidence from Jakobshavn Isbræand the North Greenland Eemian Ice Drilling facility, Greenland. Geophysics, 81(1), WA111-WA118.